ChemPhysChem

Chemistry Europe
European Chemical Societies Publishing

Accepted Article

Title: Non-Flammable Sodium Asymmetric Imide Salt-Based Deep Eutectic Solvent for Supercapacitor Applications

Authors: Joseph Chidiac, Georgios Nikiforidis, Laure Timperman, and meriem anouti

To be cited as: *ChemPhysChem* **2022**, e202200224

Link to VoR: https://doi.org/10.1002/cphc.202200224

WILEY-VCH

Non-Flammable Sodium Asymmetric Imide Salt-Based Deep Eutectic Solvent for Supercapacitor Applications

Joseph Chidiac [a], Georgios Nikiforidis[a,b], Laure Timperman [a], Mériem Anouti*[a]

(a) Laboratoire PCM2E, Université de Tours, Parc de Grandmont, 37200 Tours, France
(b) Institute for Materials Discovery, University College London, Roberts Building, Malet Place, London, WC1E 7JE

Abstract

This study reports two deep eutectic solvents (DESs) based on alkaline imide salts with asymmetric anions as functional electrolytes for supercapacitor (SC) application. The eutectic mixture of sodium (fluorosulfonyl) (trifluoromethanesulfonyl) imide (NaFTFSI) or sodium cyano-trifluoromethanesulfonyl imide (NaTFSICN) with ethylene carbonate (EC) delivers a non-flammable and stable liquid. The eutectic diagrams of the electrolytes directed to an optimal composition (w_{salt} = 0.25), hinging to that of conventional carbonate-based electrolytes, i.e., 1 mol L^{-1}. The volumetric properties of the DESs revealed a "stacking" effect, reflecting a strong coordination bond between the imide and EC anions without solvating the Na^+ cations. The DES transport properties (i.e., viscosity, conductivity, and ionicity) and temperature variations designate a high organization, similar to ionic liquids. The DESs, when coupled with activated carbon electrodes in a two-electrode symmetric configuration, yield specific capacities of 150 F g^{-1} at a normalized current density of 0.5 A g^{-1} (and 120 F g^{-1} at 2 A g^{-1}). The SC maintained 80% of its initial capacity beyond 100 h of floating at an operating voltage of 2.4 V and showed a 150 mV per hour potential loss under self-discharge. The devised eutectic mixtures offer a promising new pathway for simple, safe, and effective electrolytes for SC applications.

Keywords: deep eutectic solvent, sodium asymmetric imide salt, flammability, EDLC

* E-mail: meriem.anouti@univ-tours.fr ; https://orcid.org/0000-0002-9595-6587

Introduction

Electrochemical double-layer capacitors (EDLCs) are electrochemical energy storage devices in which electric charge is stored in the electrical double-layer formed at the interface between a polarizable electrode and an electrolyte solution when direct current voltage is applied. The electrical charges are rapidly adsorbed and desorbed without faradaic reactions. EDLCs exhibit high power density (i.e., fast power supply), almost unlimited cycle life, and require zero maintenance. This energy storage mechanism works well with activated carbon (AC) porous electrodes that manifest their functionality through micro, meso, and macropores. Among these, micropores contribute to capacitance, whereas meso and macro-pores can accelerate ion diffusion in the electrode. Activated carbon is inexpensive and has a high specific surface area (2000 $m^2 g^{-1}$) and porosity, which is advantageous for achieving high capacitance (i.e., 200 F g^{-1}).

EDLCs with a pair of ACs and an organic liquid electrolyte have been implemented as memory backup devices in electronic appliances. Still, their market applicability is limited by feeble energy densities (i.e., <10 Wh L^{-1}), stemming from the low operating cell voltage of these devices (< 3 V). To counter this limitation, newly formulated electrolytes with elongated voltage window have been reported[1]. And arguably so, as the energy of the EDLC is analogous to the square root of the SC voltage (see Equation 2 below). Taking into account the oxidative and reductive stability of electrolytes, a great deal of research on new formulations has been conducted, giving rise to ionic liquids (ILs) and deep eutectic solvents (DES) as suitable candidates for SC applications[2-6]. DESs' low cost, wide electrochemical stability window, and simplicity of formulation render them attractive in energy devices. Their most appealing feature, however, is their superionic character, which gives them transport properties (e.g., conductivity and viscosity) that are strikingly improved at elevated temperatures.

Deep eutectic media have manifested their ability to enforce strong interactions between an alkali metal salt and a compound with a high donor number[7]. To understand the formation of eutectics comprising a salt[8], we must consider interactions between the complexing agent and the salt anion. When a phase transition occurs at the eutectic point, for an ideal system, and at chemical equilibrium (i.e., $\Delta G = 0$), the Gibbs equation is represented by $T_m = \frac{\Delta H_{fusion}}{\Delta S_{fusion}}$. In reality, at the eutectic point (T_e), the entropy (S) reaches a maximum and the enthalpy (H) a minimum, described by $T_e = \frac{\Delta H_{eutectic}}{\Delta S_{eutectic}}$ [9]. What's more, the eutectic depth ΔT ($\Delta T = T_m - T_e$) depends on the organization of the mixture and the cross interactions between the mixed pure

substances. In most cases, the lowering of the melting point (i.e., eutectic depth) can reach temperatures as high as 200°C.

Several complexing agents can be utilized for DES formulation, such as amides, acids, alcohols, and even compounds with a high dielectric constant such as ethylene carbonate (EC). Subcategories of DESs are contingent on the nature of the components (metal, salt, or molecular compound)[10]. When mixing an alkali salt of an organic anion such as NaX (X denoting an imide anion) with a molecular compound that is solid at room temperature (i.e., EC), one can expect the formation of a DES due to the intrinsic properties of the latter and the tendency of imide anions to form complexes. This is the case for the asymmetric anion FTFSI. To our knowledge, there is one study that describes an eutectic mixture of an imide salt (LiTFSI) with EC for battery applications (i.e., Li metal studies)[11]. We recently reported our findings on this eutectic mixture[12] on Li metal and graphite in half-cells showing good thermal stability (C/10 rate up to 80°C), long cycling (5 months), minimal capacity fade (0.4 mAh g^{-1} per cycle for 100 cycles) and most importantly non-flammable behaviour[12]. The formation of efficient coordination bonds of the molecules of polar solvents with the Li^+ cations effectively stabilizes the free doublets of the solvent and marginalizes their sensitivity to oxidation. When less than 5% of the solvent is free and does not participate in the coordination of Li^+, the volatility of the electrolyte is markedly reduced, leading to low cell overpressure and electrolyte flammability[9].

Currently, methods for improving electrolyte properties in low temperatures include the modification of traditional organic electrolytes (i.e., optimizing solvent system) and realizing novel electrolyte salt(s). Going away from this paradigm and following a simple and effective method of devising new electrolytes, herein we present deep eutectic systems obtained by mixing asymmetric imide anion salts, either (fluorosulfonyl) (trifluoromethanesulfonyl) imide (NaFTFSI) or sodium cyano-trifluoromethanesulfonyl imide (NaTFSICN) with ethylene carbonate. We elucidate these mixtures' thermodynamic and physicochemical properties and demonstrate practical applications in laboratory-scale SCs comprising activated carbon electrodes. The devised SCs are tested using industry protocols and characterized with electrochemical techniques, such as constant-current potentiometry, floating-test, cyclic voltammetry, and electrochemical impedance spectroscopy.

Experimental Section

Electrolyte formulation

Alkyl carbonate solvents (EC: ethylene carbonate, PC: propylene carbonate, and DMC: dimethyl carbonate, >99% purity) were purchased from Sigma Aldrich and Merck (EMC: ethylene methylene carbonate) and used without further purification. The (fluorosulfonyl) (trifluoromethanesulfonyl) imide sodium salt (NaFTFSI) and N-cyano-trifluoromethane sulfonyl imide sodium (NaTFSICN) were purchased from Provisco (Czech Republic) and kept under a dry atmosphere in an argon-filled MBraun glove box (< 5 ppm moisture).

The ternary EC/PC/DMC mixture (1/1/3, wt%, η = 0.95 at 25°C) was used for comparison purposes. The eutectic mixtures were formulated by mixing EC and NaFTFSI or NaTFSICN in different mass proportions (i.e., $0 < w_{\mathrm{LiFTFSI}} < 1$). Both solid starting compounds were mixed with moderate stirring for two hours in the glove box. The relevant mass, molar fractions, and concentrations (C_{salt}, mol L^{-1}) are given in **Table 1**. C_{salt} was calculated using the density of the EC/salt mixture at 25°C. A GeneCust (France) desiccant bag was inserted in each electrolyte to reduce the water content further. The amount of residual water was determined by Karl Fisher titration (< 20 ppm). Flammability tests were carried out in ambient conditions, with the electrolytes (1.2 mL) being subjected to a flame source on top of a hot plate (WVR) operating at 200°C.

Table 1: EC/NaFTFSI and EC/NaTFSICN salt composition expressed by mass and a molar fraction (w_{salt}, x_{salt}) and molar concentration (C_{salt}).

w_{salt}	NaFTFSI		NaTFSICN	
	x_{salt}	C_{salt}	x_{salt}	C_{salt}
0	0.000	0.000	0.000	0.000
0.1	0.037	0.580	0.047	0.756
0.2	0.080	1.160	0.100	1.512
0.25	0.104	1.450	0.130	1.890
0.5	0.258	2.901	0.309	3.781
0.8	0.582	4.641	0.642	6.049
1	1.000	5.802	1.000	7.561

Physicochemical characterization of the electrolytes

The ionic conductivity measurements were performed by a BioLogic® multichannel conductometer based on a frequency response analyzer (MCM 10) that was connected to a Peltier-based temperature control unit (T_{range} = -10 to 80°C). The conductometer was pre-calibrated with a standard potassium chloride solution. The dynamic viscosity and density of the electrolytes were measured using an Anton Parr densitometer comprising a digital vibrating tube densitometer and a rolling-ball viscometer (Lovis 2000 M/ME, Anton Parr, France). The densitometer/viscometer was pre-calibrated with ultra-pure water. Differential scanning calorimetry was performed with a PerkinElmer DSC 4000 calorimeter. The samples were initially cooled to -60°C, followed by a five-minute isothermal plateau at this temperature, then heated up to 250°C at a scan rate of 5°C min^{-1}. The dimensions of species (EC, Na-EC, FTFSI, TFSICN) were calculated using density functional theory (DFT) by geometry optimization with the B3LYP functional and 6- 311 + G(d) basis set (Gaussian - Hartree-Fock theory).

Material characterization

Activated carbon (AC, Blue Solution, France) coated on aluminum was the electrode of choice for the positive and negative electrodes of the SC. The physicochemical and textural parameters of the AC have been described in a previous report[13]. A four-point probe system (Ossila) calculated the sheet resistance and conductivity of the AC electrodes before and after cycling. An average of 100 readings is reported here. The AC thickness (76 μm ±3 μm) was determined by a profilometer (Dektat XT). The Raman spectra were obtained inVia™ confocal Raman microscope (Renishaw) under a 532 nm laser excitation and a 10× magnification lens. The deconvolution of the D and G bands was done by Lorentzian fitting.

Supercapacitor assembly

The activated carbon electrodes had a diameter of 1 cm (geometric surface area of 0.7854 cm^2). The separator (Whatman filter paper, GF/C, ϕ = 12 mm) was dried in a Buchi oven at 80°C for 12 h and transferred to the glovebox with no exposure to air. An electrolyte volume of 300 μL was used for the SCs. After the SC assembly, the cells remained at open circuit for 12 h at room temperature for adequate wettability and equilibration.

Electrochemical characterization

The galvanostatic charge-discharge (GCD), floating, cyclic voltammetry (CV), and potentiostatic electrochemical impedance spectroscopy (PEIS) measurements were carried out by a Biologic potentiostat (Biologic, France). PEIS was conducted between 0.15 MHz and 10

mHz, at open-circuit voltage with an AC perturbation of 10 mV. CV plots were performed relative to the set electrochemical window at designated scan rates (1-100 mV s^{-1}) and normalized with respect to the active mass of the activated carbon (i.e., ~0.05 mg). The floating protocol was initiated with five initial GCD cycles at 0.5 A g^{-1} between the set electrochemical window (either U_{max} = 2.4 or 2.0 V), followed by a potentiostatic step at U_{max} for 1.5 h and followed by five final GCD cycles[14]. This sequence was repeated for a set amount of hours, typically 100. All SC devices were cycled under ambient conditions. The specific capacitance (C_{sp}, F g^{-1}) of the SC was determined by the following Equation[15, 16]:

$$C_{sp} = \frac{1000}{m \times v \times (E_+ + E_-)} \int_{E_-}^{E_+} I(V)dV \qquad \text{Equation 1}$$

where m represents the active mass on one electrode (mg), v is the scan rate (mV s^{-1}), E_+ and E_- denote the cathodic and anodic potentials (V), respectively, and I connotes the current response (mA). For the Ragone plot, the energy (E, Wh kg^{-1}) and power (P, W kg^{-1}) of the SC are given by the following equations:

$$E = \frac{1}{2} \times C_{smax} \times (U_{max})^2 \qquad \text{Equation 2}$$

$$P = \frac{(U_{max})^2}{4 \times m \times R_{cell}} \qquad \text{Equation 3}$$

where $U_{max.}$ denotes the maximum cell voltage the SC operates under, C_{max} represents the maxim specific capacitance of the SC, m is the mass of the active material, and R_{cell} describes the SC internal resistance.

Results and Discussion

Thermal characterization and eutectic diagram

The adiabatic eutectic diagrams of the binary mixtures are given in **Figures 1a** and **1b**. The thermograms of EC with NaFTFSI and NaTFSICN range between -60 and 250°C for several compositions (i.e., 20/80 → 90/10, EC/salt). The mass fraction of salt (w_{sal}) lies between zero and one (**Table 1**). The pure compounds (EC, NaFTFSI, and NaTFSICN) display melting temperatures consistent with those observed in the literature, viz. $T_{m\ EC}$ = 36°C [17], $T_{m\ NaFTFSI}$ = 141°C [18] and $T_{m\ NaTFSICN}$ = 260°C. The asymmetric salts containing the $TFSICN^-$ anion, which has the greatest asymmetry, exhibited the highest melting temperature for the two sodium salts. The eutectic points of the devised electrolytes expressed in molar fraction (x_{salt}, T_e) are illustrated in **Figures 1c** and **1d**. The eutectic point for the EC/NaTFSICN solution lies at 0.2, for the EC/NaTFSI mixture at 0.14, while for EC/LiTFSI it reaches 0.4[12]. The lower eutectic

point of Na-based DESs indicates that the size, charge density, and polarizability of the Na^+ cation induce less interaction with anions, rendering the formation of the EC-anion complex facile. **Table 2** summarizes the thermodynamic characteristics, including the eutectic composition (x_e, T_e) and depth (ΔT) of the Na-imides salt-based mixtures against a Li analog, i.e., EC/LiFTFSI[12].

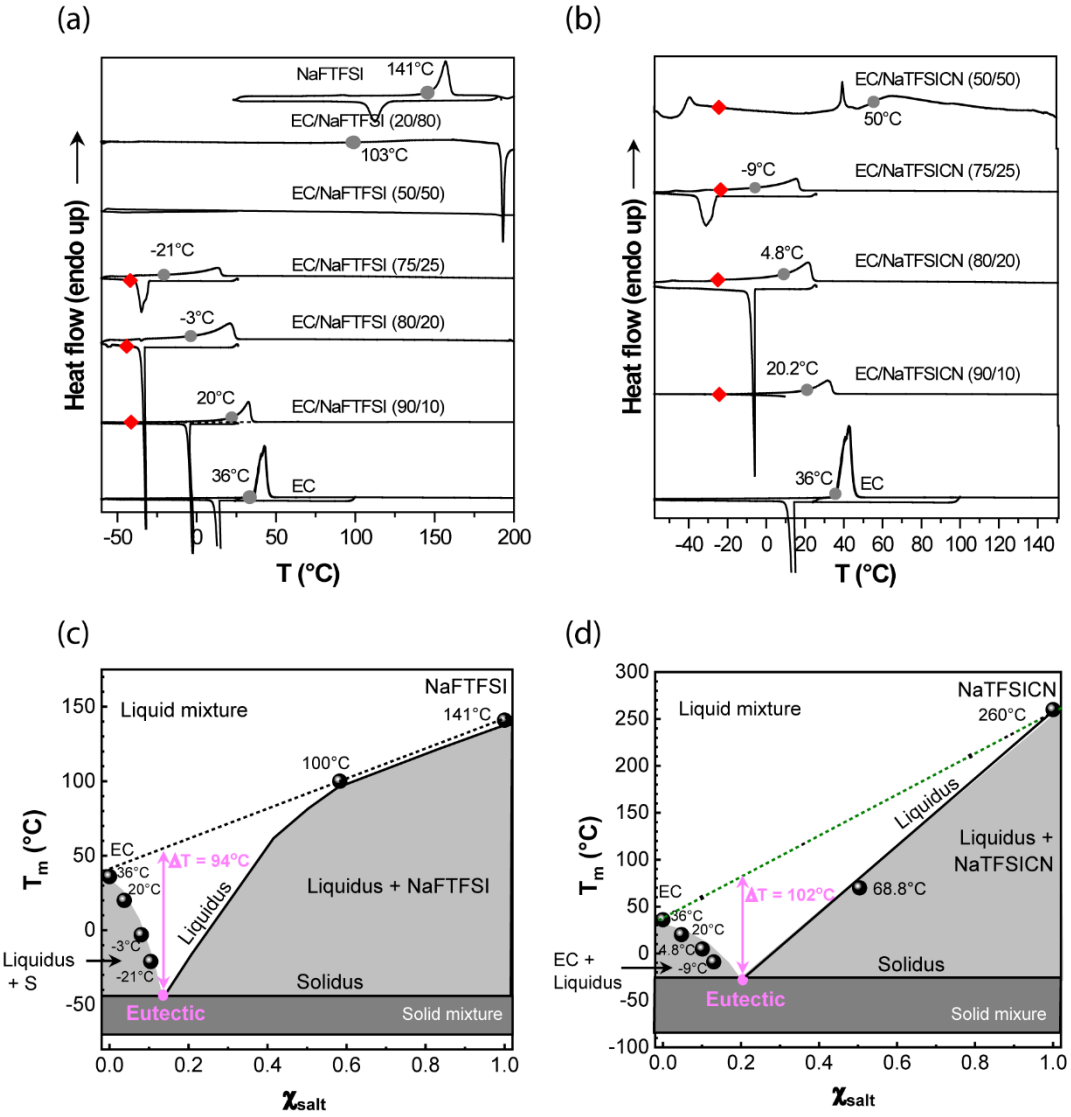

Figure 1 Thermograms of (a) (EC/NaFTFSI) and (b) (EC/NaTFSICN) mixtures at different weight compositions. The red squares denote the solidus. The grey circles denote the point of liquidus. Eutectic diagram of binary mixtures (c) NaFTFSI/EC and (b) NaFTFSICN/EC as a function of the molar fraction of FTFSI (x_{salt}). The dotted lines (grey and green) describe the melting of an ideal system.

The eutectic depth corresponds to the difference between an ideal behavior (depicted by the purple line in **Figures 1c** and **1d**) and the actual mixture obtained. Here, it lies between 90 and 105°C. Depending on the nature of eutectic mixtures (i.e., composition), eutectic depths

range between 70 and 300°C and are categorized into different classes[10]. The calculated eutectic depth designates the investigated DES into Type III, similar to quaternary ammonium salt and hydrogen bond donor. Yet, it should be noted that Abbott's classification of DES[10] does not include complexing agents of the molecular solvent type with a high dielectric constant, such as EC.

Table 2 Thermodynamic characteristics of eutectic mixtures containing EC and asymmetric imide anion salts, NaFTFSI, and NaTFSICN. A Li-based eutectic analogue is presented here for comparison purposes.

Eutectic	EC/NaFTFSI	EC/NaTFSICN	EC/LiFTFSI[12]
$T_{m\ salt}$ (°C)	141	260	91
x_e (molar fraction)	0.15	0.20	0.40
T_e (°C)	-40	-25	-25
ΔT	90	104	94

Taking into account the eutectic diagrams of **Figures 1c** and **d**, we proceeded with eutectic mixtures having a relatively low mass fraction (i.e., w_{salt} = 0.25), corresponding to a salt concentration between ~1.5 and 1.9 mol L^{-1} (**Table 1**). Highly concentrated electrolytes (HCE) are more electrochemically stable; at the same time, they are costly and viscous[11]. With w_{salt} set at 0.25, the studied DESs, as demonstrated in the section below, show good transport properties (σ, η, ρ) for SC applications.

Physical properties of eutectic electrolytes EC/NaFTFSI and EC/NaTFSICN

Volumetric properties

The changes in electrolyte density (ρ) between 10 and 55°C are shown in **Figure 2a**. The eutectic mixtures are moderately denser (1.45<ρ<1.5 g cm^{-3}) than standard carbonate-based electrolytes such as EC/EMC (3/7 wt) and 1 mol L^{-1} NaFTFSI (or 1 mol L^{-1} NaTFSICN) whose density lies between 1.1 and 1.3 g cm^{-3} at 25°C[19, 20]. The compactness of the eutectic mixtures leaves little free volume, making them denser. With the aid of empirical relationships (Equations 4 and 5), together with Glasser's theory [24] (Equations 6 and 7), we model the density variation with temperature. The results are given in **Table 3**.

$$\alpha = -\left(\frac{\partial \ln(\rho)}{\partial T}\right)_p \quad \text{Equation 4}$$

$$V_m = \frac{M}{\rho \mathcal{N}} \quad \text{Equation 5}$$

$$S^0 = 1246.5\, V_m + 29.5 \qquad \text{Equation 6}$$

$$U_{pot} = 1981.2 \left(\frac{\rho}{M}\right)^{1/3} + 103.8 \qquad \text{Equation 7}$$

where α represents the coefficient of thermal expansion that reflects the ability to restructure solutions under thermal agitation. V_m describes the molecular volumes of the mixtures while S^0 *and* U_{pot} depict the standard molar entropy and crystal energy of the mixtures according to Glasser's theory.

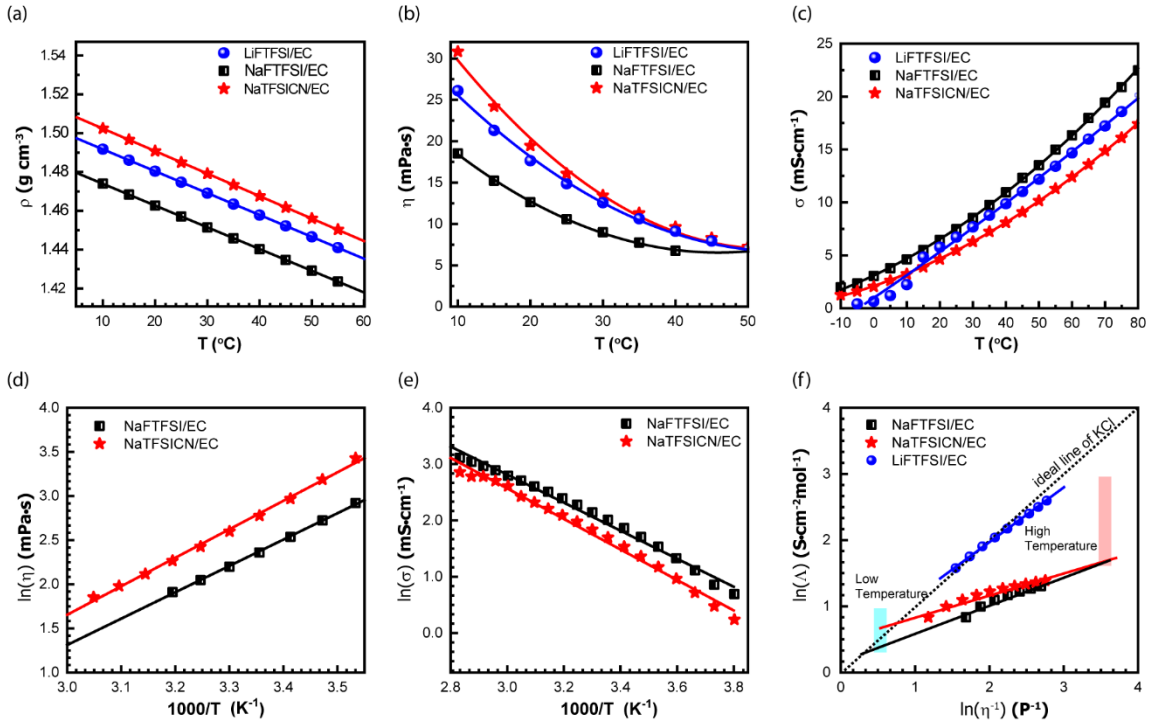

Figure 2 Variation of (a) density, (b) viscosity, and (c) conductivity with temperature for the eutectic electrolytes NaFTFSI/EC and NaTFSICN/EC. w_{salt} is equal to 0.25. Arrhenius plot of viscosity (d) and conductivity (e). Walden curves for ionicity evaluation of the NaFTFSI/EC and NaTFSICN/EC eutectic mixtures. The LiTFSI/EC plots are used for comparison purposes and taken from[12].

The tabulated volumetric coefficients of expansion (α) lie between those of organic solvents (i.e., $4\times10^{-4} < \alpha < 7\times10^{-4}$; K^{-1})[19, 21-23] and ionic liquids (i.e., $8\times10^{-4} < \alpha < 10\times10^{-4}$; K^{-1})[24, 25], suggestive of systems containing self-associated molecules[26]. Generally, the DESs molar volume values range from 72 to 264 $cm^3\ mol^{-1}$ [27]. The calculated molecular volumes here vary between 77 and 88 cm^3, in the lowest range of the DESs category. The intermolecular interactions between the EC and the anions promote self-association domains by stacking in liquid networks[28], called the "stacking" effect[29].

Table 3 Volumetric and thermodynamic properties of the eutectic electrolytes NaFTFSI/EC and NaTFSICN/EC at 25°C. Coefficient of thermal expansion, α (K^{-1}), crystal energy, U_{pot} (kJ mol^{-1}), and standard molar entropy $S°$ (J mol^{-1} K^{-1}).

Eutectic	NaFTFSI/EC	NaTFSICN/EC
10^4 α (K^{-1})	-7.74	-7.87
V_m (cm^3 mol^{-1}) at 25°C	88.48	77.45
$S°$ (J mol^{-1} K^{-1})	217.7	194.4
U_{pot} (kJ mol^{-1})	544.4	564.3

The NaTFSI/EC mixture exhibits the lowest organizational entropy and highest crystal energy U_{pot}. Low values of U_{pot} reflect a structured organization in the liquid state and low S^0 values indicate interaction sensitivity between species within temperature variations[23]. The eutectic mixtures are less organized than their homologue standard electrolytes based on LiFTFSI salt (i.e., $S°$ = 209 J mol^{-1} K^{-1} and U_{pot} = 550 kJ mol^{-1})[12] and seem to promote self-association domains by comparison with standard electrolytes.

Viscosity and conductivity of eutectic mixtures

The variations in dynamic viscosity and conductivity of the NaFTFSI/EC and NaTFSICN/EC mixtures are given in **Figure 2b**. The more pronounced viscosities are found at low temperatures, viz. 10°C for the NaTFSICN/EC mixture (30.83 mPa·s), ×2.5 higher than that of NaFTFSI/EC (18.53 mPa·s) owing to the larger TFSICN ion. Elevated temperatures improve the ions' mobility, leading to a decrease in viscosity (i.e., $\eta_{\text{NaFTFSI/EC 50C}}$ = 7.24 mPa·s). When compared to values of standard carbonate electrolytes based on asymmetric imide salts at similar concentrations (~1.4 mol dm^{-3}), they are ×8.0 larger[30] (**Table 1**). Still, this viscosity range is not prohibitive for SC applications.

The ionic conductivity of NaFTFSI/EC is more significant than the one for NaTFSICN/EC throughout the investigated temperature range (**Figure 2c**, σ = 7.48 vs. 5.46 mS·cm^{-1} at 25°C). Eutectic mixtures are not as conductive as other liquids (e.g., aqueous electrolytes) due to the coordination bonds that characterize them. At elevated temperatures, the NaFTFSI/EC mixture displays its highest conductivity (16.34 mS·cm^{-1}) close to one containing 1 mol L^{-1} LiFTFSI in EC/PC/3DMC.

Table 4 Viscosity (η) and conductivity (σ) for LiFTFSI/EC, NaFTFSI/EC, and NaTFSICN/EC mixtures at different temperatures. nd denotes not determined

Electrolyte	Viscosity (mPa·s)			Conductivity (mS·cm^{-1})		
	10°C	25°C	50°C	10°C	25°C	50°C
NaFTFSI/EC	18.53	10.58	8.87	4.63	7.48	16.34
NaTFSICN/EC	30.83	16.08	7.24	3.23	5.46	12.41
1 mol L^{-1} LiFTFSI (EC/PC/3DMC)	4.27	3.03	1.85	8.32	11.25	20.47

It should be noted that the transport properties of the eutectic mixtures are ×4 more viscous and ×2 less conductive than the standard electrolyte, suggesting, at first instance, a hindered SC performance. Yet, this is not the case since the ionic mobility is moderately affected by the viscosity. What's more, such a comparison is distorted by the ion composition of the two media. Standard electrolytes typically have an ionic concentration of 1.0 mol L^{-1}, whereas DESs are richer in ions (i.e., the concentration reaches 1.9 moL L^{-1}, **Table 1**), favoring EDL formation. To this end, if fluidity and concentration are taken into account, their ionicity appears comparable at low temperatures to that of standard electrolytes, including KCl, as depicted by the Walden curve of **Figure 2f**.

Modeling and fitting parameters

An Arrhenius-type relationship is introduced to delineate the transport phenomena of these eutectic mixtures. The activation energies E_a^{η} and E_a^{σ} are extracted from the slopes of **Figure 2d** and tabulated accordingly. The E_a^{η} values reveal that the energy barrier of the viscous flow is 41% higher than the ones containing conventional ternary or binary solvent mixtures (e.g., EC/PC/3DMC or 3EC/7EMC)[20, 30], signifying stronger intermolecular interactions. This may be because only EC ensures the solvation of Na^+ and the complexation of imide anions. The presence of linear carbonates in standard electrolytes loosens the interactions and increases the fluidity of the mixture.

Based on Eyring's theory, viscous flow can be regarded as an activated process[31], which relates transport properties to thermodynamic models. In this regard, the excess free Gibbs energy of activation for the flow process ($\Delta G^{\neq}$) can be expressed by a thermodynamic excess free Gibbs energy. The Gibbs energy variation for the activated state $\Delta G^{\neq}$, ($\Delta G^{\neq} = \Delta H^{\neq} - T\,\Delta S^{\neq}$) is modeled as a quasi-lattice where the moving molecules reach an activation energy before

jumping into an available empty site (i.e., hole)[23]. Under these circumstances, the viscosity of a liquid mixture is given by:

$$\eta = \frac{h\mathcal{N}_A}{V_m} exp\left(\frac{\Delta S^{\neq}}{R}\right) + exp\left(\frac{\Delta H^{\neq}}{RT}\right) \quad \text{(Equation 8)}$$

where h, $\mathcal{N}_A$, R are physical constants, and T the absolute temperature. The molar volume of the solution, V_m stems from the solution density. The transition state entropies, $\Delta S^{\neq}$ are extracted from the intercept of $\ln(\eta) = f\left(\frac{1}{T}\right)$ for the eutectic and conventional systems and reported in **Table 5**. The low $\Delta S^{\neq}$ values highlight the presence of anion-EC-cation associations that reduce the freedom of moving species in the solution. Thus, the occupation of "free holes" becomes more complex, leading to high entropy and activation values since they need to be surpassed before reaching the available holes.

Table 5 Activation energies (E_a^{η} and E_a^{σ}) and entropies related to dynamic viscosities for the eutectic mixtures NaFTFSI/EC and NaTFSICN/EC. A standard carbonate-based electrolyte containing the same salts is used for comparison purposes.[20]

	Electrolyte	$E_a^{\eta} \pm 0.05$ (kJ mol^{-1})	$\Delta S^{\neq} \pm 0.1$ (J mol L^{-1})	$E_a^{\sigma} \pm 0.05$ (kJ mol^{-1})
Salt + EC	1.4 mol L^{-1} NaFTFSI	24.83	36.77	20.70
	1.9 mol L^{-1} NaTFSICN	26.84	31.32	22.52
Salt + EC/PC/3DMC	1 mol L^{-1} NaFTFSI	14.38	59.94	12.60
	1 mol L^{-1} NaTFSICN	13.99	62.29	13.28

The conductivity and viscosity of a liquid are often combined into Walden's rule. The Walden plot describes the relationship between conductivity and viscosity of pure ionic liquids (ILs) and evaluates the extent of ion association[32]. Equations 9 and 10 refer to the Walden product ($W = \Lambda.\eta$) [2].

$$(\Lambda.\eta)^{\alpha} = \mathrm{B} \quad \text{(Equation 9)}$$

$$\log(\Lambda) = \log(\mathrm{B}) + \alpha \times \log(\eta^{-1}) \quad \text{(Equation 10)}$$

where Λ is molar conductivity, η the viscosity, and B is a constant. From **Equation 9**, α is a correlation factor that describes the dissociation rate [32]. When α equals to 1, the ion

mobility is solely governed by the solution fluidity. When $\alpha \neq 1$, the viscous flux is no longer fully responsible for ion mobility. The linear curves of **Figure 2f** meet the ideal KCl line (1 mol L^{-1} KCl) at 25°C. Hence, the NaFTFSI/EC and NaTFSICN/EC eutectic systems, located further from the KCl line than EC/LiFTFSI, are less dissociated and, therefore, less ionic. This difference is accentuated at higher temperatures.

Flammability tests of eutectic mixtures

Flammability tests were carried out for the NaFTFSI/EC eutectic mixture and compared to the conventional electrolyte comprising EC/PC/3DMC and 1 mol L^{-1} LiFTFSI. The eutectic combination does not show any signs of ignition after prolonged exposure to flame (i.e., 50 seconds, **Figure 3**) in contrast to the conventional electrolyte (within 5 seconds), corroborating its non-flammable nature. We postulate that the non-flammability stems from i) the absence of linear alkyl carbonates such as DMC that have a low flash point (17°C), and ii) the strong coordination of the anion by the EC.

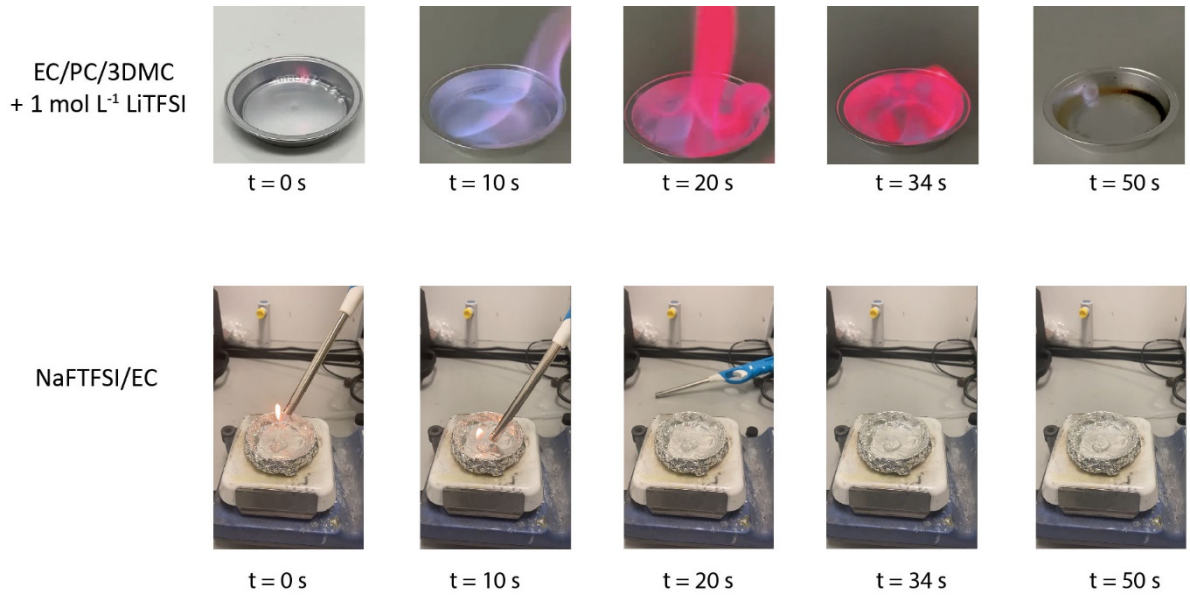

Figure 3. Electrolyte flammability of EC/PC/3DMC LiTFSI and NaFTFSI/EC electrolytes. 1.2 mL of electrolyte was subjected to a flame to initiate direct combustion in an aluminum capsule while monitoring the extinction time.

Electrochemical characterization of eutectic mixtures for SC application

The electrochemical window of the electrolytes was determined by cyclic voltammetry at a low scan rate (1 mV s^{-1}). The Swagelok-type cell comprising activated carbon electrodes with an Ag wire as a pseudo-reference electrode showed an operating window of 2.4 V (**Figures 4a** and **4b**) for both eutectic mixtures, on par with other symmetric SCs based on AC [2,13]. Conventional galvanostatic charge-discharge cycling better resembles real device operation, and thus its use is essential for practical purposes. For normalized current densities spanning from 0.5 to 5 A g^{-1} (**Figures 4c** and **4d**), we obtained triangular charge-discharge curves typical of an EDLC[15]. Still, the deformed shape of the rectangle at 2.4 V (i.e., fill factor = 78%) is more pronounced for the NaTFSICN/EC electrolyte due to cell polarization coming from the the $C \equiv N$ bond of the $TFSICN^-$ anion. The charge-discharge specific capacities translated from the cyclic voltammetry plots (i.e., by integrating $i = f(t)$), are given in **Table 6**.

10.1002/cphc.202200224

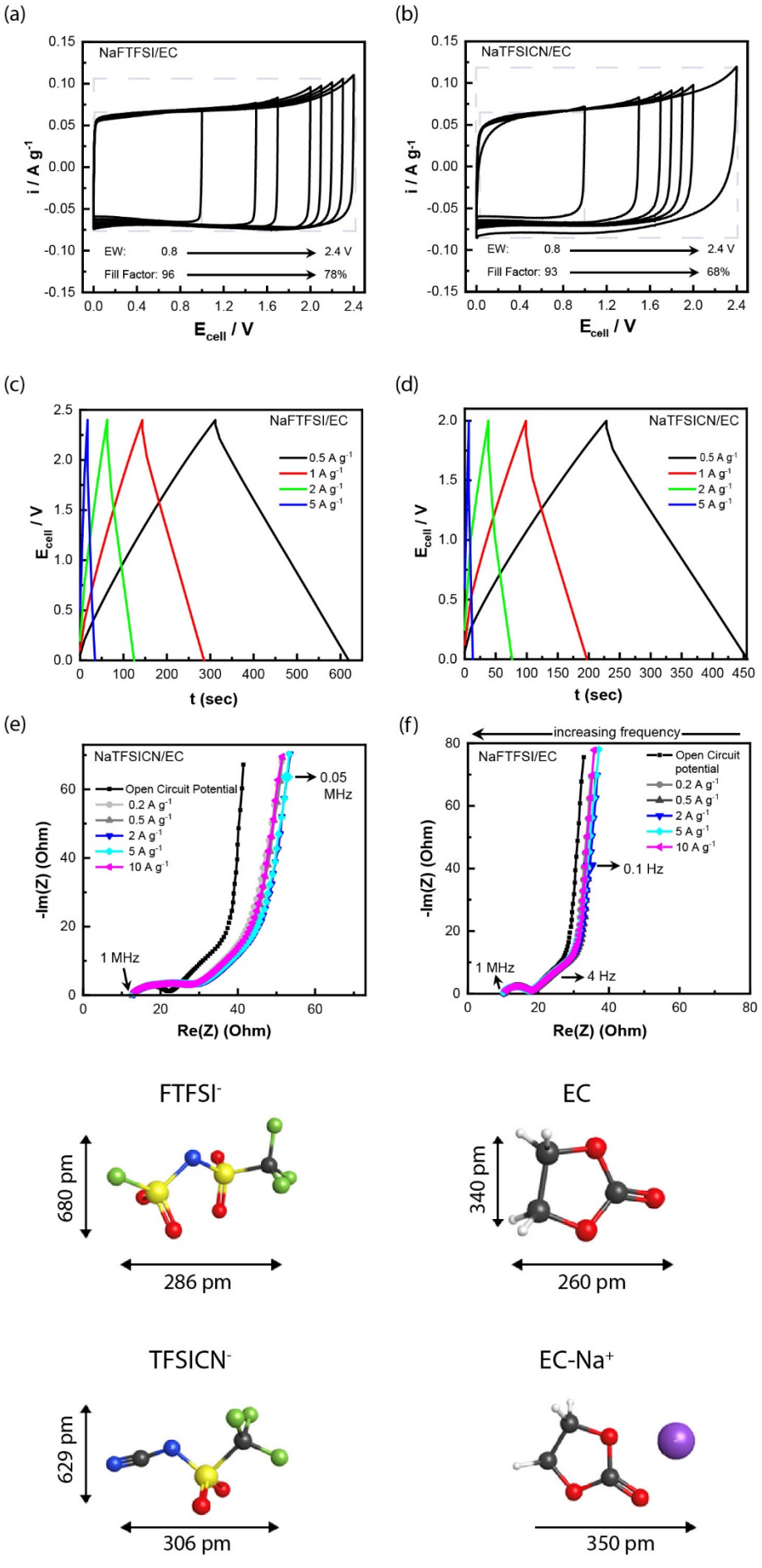

Figure 4. Cyclic voltammograms (a,b), galvanostatic charge/discharge profiles (c,d), and Nyquist plots (e,f) carried out in symmetrical supercapacitor based on activated carbon for the NaFTFSI/EC and NaTFSICN/EC eutectic mixtures at room temperature. The schematic below depicts the dimensions of the complexes (i.e., length and width). For the case of EC—Na^+, the diameter dimension is provided.

Table 6 Specific capacity stemmed from the cyclic voltammetry plots on a three-electrode Swagelok-type cell containing the NaFTFSI/EC and NaTFSICN/EC electrolytes. The operating temperature is 25°C. Scan rate is 1 mV s^{-1}.

Electrolyte	Operating Voltage (V)	Charge Capacity (F.g^{-1})	Discharge Capacity (F.g^{-1})	Coulombic Efficiency (%)
NaFTFSI/EC	2.4	143.8	137.9	96
NaTFSICN/EC	2.0	142.8	138.2	97
NaTFSICN/EC	2.4	180.5	165.4	91

Cycling above the lower stability limit (2.0 V) for the NaTFSICN/EC eutectic mixture lowers the coulombic efficiency (3% decrease for a 400 mV shift; 2.0 → 2.4 V). We postulate that ions adsorbed on the activated carbon surface during the charge do not readily diffuse upon discharge (i.e., ions are trapped in the micropores of the electrode). Indeed, the activated carbon used in this study has a specific surface area of 1511 m^2 g^{-1}, pore volumes reaching 0.691 cm^3 $g^{-1,}$ and a large number of micropores ($\phi \leq$ 1 nm)[13,33]. The dimensions of the species comprising the eutectic mixtures are given in the schematic of **Figure 4** and are lower than the microporosity of activated carbon.

The Nyquist plots before and after the imposition of the current densities are displayed in **Figures 4e** and **4f**. The breakout of the Nyquist plot and its equivalent circuit ($R_{ESR} + C_{dl}/(R_{CT}$ + W) + C_{FD}/R_{np})) has been previously reported[13]. The bulk ionic conductivity is highly associated with the equivalent series resistance (R_{ESR}) and is extracted at high frequencies (>20 kHz). R_{ESR} is typically connected in series with the double layer capacitance (C_{dl}) that describes the eutectic mixtures' ionic and activated carbon's electronic charges. The capacitance lies in parallel with the charge transfer resistance (R_{CT}) that is portrayed by the semi-circle within the high to middle frequencies (1 MHz - 1 kHz). The broad semi-circle is followed by a 45° line, characteristic of the ion diffusion in the electrode's pores, assuming semi-infinite linear diffusion[34]. The near-vertical line at low frequencies (e.g., 0.05 Hz) verifies the ideal capacitive behavior of the SC (i.e., finite diffusion)[13]. A final resistive element (R_{np}) is associated with the

non-ideal polarizable capacitance. The values extracted from the Nyquist plots at the open circuit potential and the maximum operating potential (E_{max}) are given in **Table 7.** The NaTFSICN/EC eutectic mixture shows resistances ×1.5 larger than NaTFSI/EC, owing to the asymmetric structure of this anion. The $C \equiv N$ group strongly adsorbs to the surface of the activated carbon and hinders diffusion within the more viscous electrolyte (i.e., 20 vs. 12 mPa·s, **Figure 2b**).

Table 7 Calculated resistances from the Nyquist plots of **Figure 4e** and **4f** before and after cycling at the open-circuit voltage (OCV) and maximum operating cell voltage (E_{max} = 2.4 V) for the SCs comprising NaFTFSI/EC and NaTFSICN/EC electrolytes.

Resistance (Ohm)	NaFTFSI/EC		NaTFSICN/EC	
	OCV	2.4 V	OCV	2.4 V
R_{ESR}	9.95	9.84	14.76	14.26
R_{CT}	5.58	4.73	15.17	17.06
R_{np}	15.63	15.24	29.03	30.83

The GCD curves of the SCs comprising the eutectic mixtures at different operating potential windows (viz. 0.5-2.4 V) for a set normalized current density of 200 mA g^{-1} are presented in **Figures 5a** and **5b**. There is an increase in their specific capacity with an elongated operating window, reaching 148 F g^{-1} at 2.4 V for the case of NaFTFSI/EC (**Figure 5c**). In addition, the voltage drop (ΔU) verified at the charge-discharge transition for the applied current (I) is used in conjunction with Ohm's law to obtain the R_{ESR} (e.g., $R_{ESR} = \Delta U/\Delta I$). The R_{ESR} values complement the ones in **Table 7** (10 Ohm ± 0.23 for the SC comprising NaTFSI/EC) and remain constant with voltage increase. The NaFTFSI/EC mixture performs better and retains 90 F g^{-1} at a normalized current density of 5 A g^{-1}, twice as high as the SC comprising NaTFSICN/EC (**Figure 5d**). Higher currents amend the effective thickness (here acting as a separator of dissolved ions) and morphology of the ECDL (i.e., fewer ions can occupy the activated carbon inner spaces), leading to lower charge storage. An example of a GCD curve is given in **Figure 5e** at 2 A g^{-1} for 8 h. Self-discharge curves of the same cell are illustrated in **Figure 5f** at different charing times (i.e., amperometry at 2.4 V for 1 to 10 minutes). The open circuit of the SC reached 1.0 V after 10 h, with a 150 mV decrease per hour.

Furthermore, accelerated aging floating tests[20, 35] were initiated to evaluate the stability of the SCs during long-term cycling. The tests were conducted within a voltage window of 0 to 2.4 V for the NaFTFSI-based electrolyte (**Figure 5g**) and 0 to 2.0 V for the NaTFSICN-based electrolyte. The specific capacity retention reaches 80% for 100 h of floating. Beyond this timeframe, the capacity decreases in a linear fashion, reaching 50 F g^{-1} at 300 h. The mean sheet resistance and conductivity of the AC electrodes before and after floating are recorded. In a pristine state, the mean sheet resistance of the AC (i.e., an average of four different locations on the electrode) reaches 1.17 Ohm/□ (±0.064), and its conductivity was equal to 1.4×10^4 S·m ($\pm 3.1 \times 10^3$). After floating, the mean sheet resistance increased six-fold to 6.085 Ohm/□ (±0.029), and the mean conductivity decreased to 2.3×10^3 S·m (±9.1). The resilience of the activated carbon on the eutectic mixture is also evident in the acquired Raman spectra. **Figure 5i** shows the D and G bands at 1349 and 1580 cm^{-1}, respectively. The G band characterizes the disorder-induced mode and in-plane stretching of all pairs of sp^2 carbon atoms, while the D band describes defects related to sp^3 carbons located in the sp^2 carbon crystal lattice[36]. The D/G band intensity for the pristine sample is ca. 1.27, indicative of the presence of sp^2 domains. After the floating process, the I_D/I_G ratio increased to 1.33, leading to a greater number and/or size of sp^2 clusters. The Ragone plots for the SCs comprising the two eutectic mixtures are on par with SC comprising organic [4, 20, 37] media and superior to SCs with aqueous[38-41] and DES media[24,26,27].

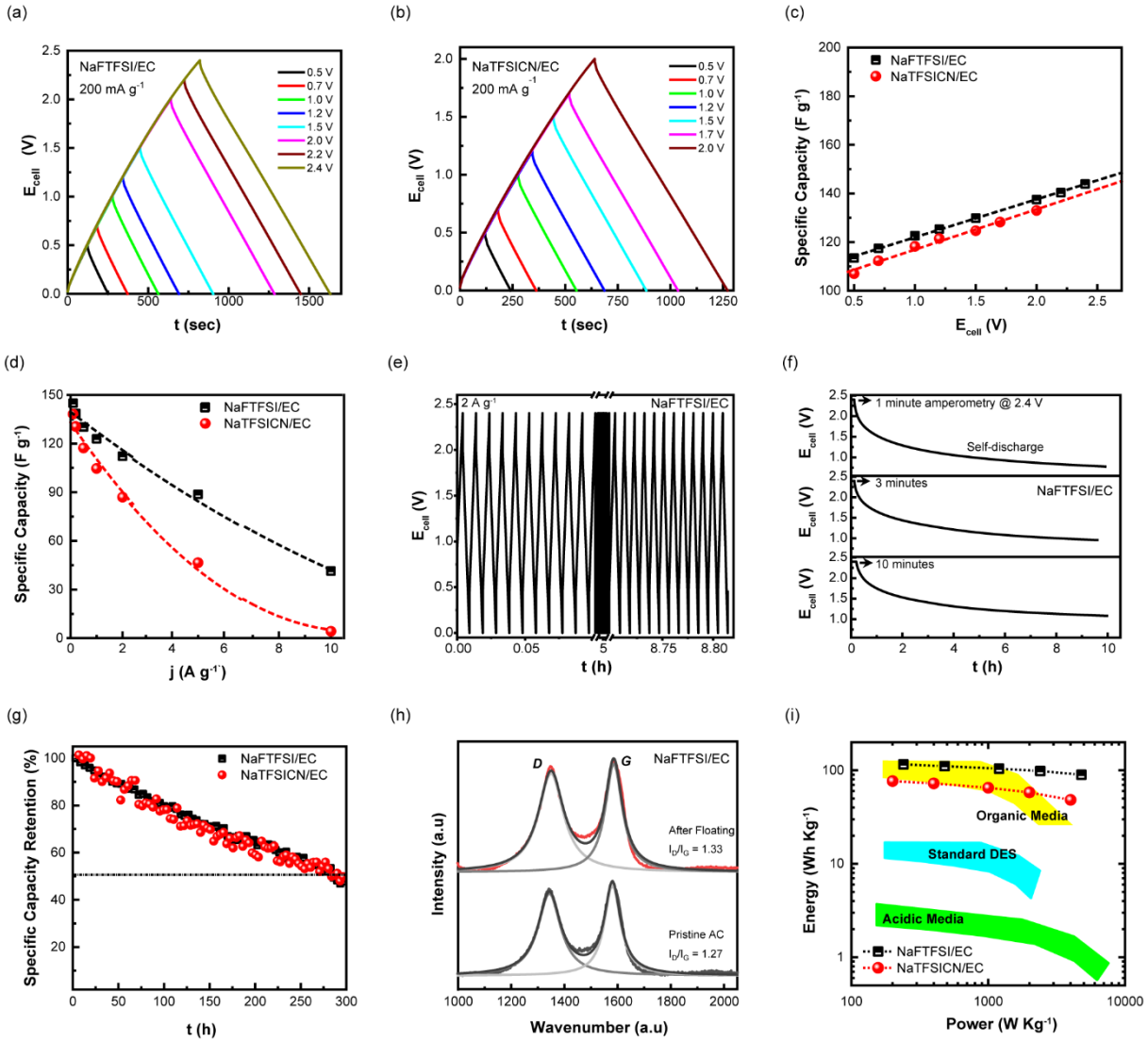

Figure 5. (a, b) Galvanostatic charge/discharge profiles for the eutectic mixtures under j = 200 mA g^{-1}. (c) Specific capacity as a function of operating voltage. (d) Specific capacity as a function of applied current density. (e) Galvanostatic charge/discharge profile of the NaFTFSI/EC at 2 A g^{-1}. S (f) Self-discharge curve of the SC under open-circuit condition for 10 h after being charged at 2.4 V for 1, 3, and 10 minutes. (h) Specific capacity retention during the floating process. (h) Raman spectra of the activated carbon electrodes with the deconvolution of D and G peaks before and after use. (i) Ragone plots for the studied eutectic mixtures compared to peers.

Conclusion

This study presents two new eutectic mixtures comprising asymmetric imide anion salts, NaFTFSI, and NaTFSICN, with ethylene carbonate. The eutectic diagrams indicate that the devised electrolytes behave like deep eutectic mixtures. The analysis of the volumetric properties revealed the nature of the interactions between EC-anion and cation where the "stacking" effect or self-association domain (i.e., efficient stacking of the liquid network) is manifested. The variations in viscosity and ionic conductivity with temperature suggested the activation energies (E_a^{η} & E_a^{σ}) follow a Grötthuss-type diffusion mechanism where the energy barrier depends on the nature of the salt. Their low charge density and polarizability induce fewer interactions with $FTFSI^-$, rendering the formation of the EC-FTFSI complex easy.

The selected composition for SC testing (i.e., NaFTFSI/EC_n; n = 10) is a compromise between the temperature of the liquid zone, the optimum transport properties, and salt composition (1 mol L^{-1}), allowing us to directly compare the devised electrolytes with typical carbonate-based electrolytes such as EC/PC/3DMC. Standard electrochemical tests (e.g., specific capacity retention reaches 80% for 100 h of accelerated aging floating tests, loss of 150 mV per hour under self-discharge test) performed on symmetric two-electrode SCs showed similar performances to organic solvents comprising imide salts (Ragone plot, **Figure 5i**). The activated carbon shows increased sheet resistance, and the Raman spectra corroborate the increased number of sp^2 clusters. Overall, the outstanding trait of these novel eutectic electrolytes based on sodium salt is their binary formulation's simplicity and non-flammable nature that predisposes them to be robust and safe electrolytes for SC applications.

Acknowledgments

The authors would like to thank "La Région Centre Val de Loire" for financial support.

Declaration of Competing Interest

The authors declare that they have no known competing financial interests or personal relationships that could have appeared to influence the work reported in this paper.

Data availability. Data that supports the findings of this study are available within the article.

References

[1] J. Yang, J. Liu, Y. Chen, B. Chang, X. Zhang, X. Wang, *ACS Appl. Energy Mater*. **2021**, *4*, 13766-13775.
[2] S. Amara, W. Zaidi, L. Timperman, G. Nikiforidis, M. Anouti, *J. Chem. Phys.* **2021**, *154*, 164708.
[3] S. Phadke, S. Amara, M. Anouti, *ChemPhysChem*. **2017**, *18*, 2364-2373.
[4] W. Zaidi, L. Timperman, M. Anouti, *RSC Adv.* **2014**, *4*, 45647-45652.
[5] W. Zaidi, A. Boisset, J. Jacquemin, L. Timperman, M. Anouti, *J. Phys. Chem. C*. **2014**, *118*, 4033-4042.
[6] T. Wang, J. Guo, Y. Guo, J. Feng, D. Wu, *ACS Appl. Energy Mater*. **2021**, *4*, 2190-2200.
[7] A. P. Abbott, D. Boothby, G. Capper, D. L. Davies, R. K. Rasheed, *J. Am. Chem. Soc.* **2004**, *126*, 9142-9147.
[8] M. H. Chakrabarti, F. S. Mjalli, I. M. AlNashef, M. A. Hashim, M. A. Hussain, L. Bahadori, C. T. J. Low, *Renew. Sustain. Energy Rev.* **2014**, *30*, 254-270.
[9] D. Yu, Z. Xue, T. Mu, *Chem. Soc. Rev.* **2021**, *50*, 8596-8638.
[10] E. L. Smith, A. P. Abbott, K. S. Ryder, *Chem. Rev.* **2014**, *114*, 11060-11082.
[11] V. Nilsson, A. Kotronia, M. Lacey, K. Edström, P. Johansson, *ACS Appl. Energy Mater*. **2020**, *3*, 200-207.
[12] J. Chidiac, L. Timperman, M. Anouti, *Electrochim. Acta*. **2022**, *408*, 139944.
[13] G. Nikiforidis, M. E. Yagoubi, M. Anouti, *Electrochim. Acta*. **2022**, *402*, 139529.
[14] L. Timperman, A. Vigeant, M. Anouti, *Electrochim. Acta*. **2015**, *155*, 164-173.
[15] G. Nikiforidis, S. Wustoni, D. Ohayon, V. Druet, S. Inal, *ACS Appl. Energy Mater.* **2020**, *3*, 7896-7907.
[16] G. Nikiforidis, S. Wustoni, C. Routier, A. Hama, A. Koklu, A. Saleh, N. Steiner, V. Druet, H. Fiumelli, S. Inal, *Macromol. Biosci.* **2020**, *20*, 2000215.
[17] O. G. Reznitskikh, A. S. Istomina, S. S. Borisevich, E. Y. Evshchik, E. A. Sanginov, O. V. Bushkova, Y. A. Dobrovolsky, *Russ. J. Phys. Chem. A.* **2021**, *95*, 1121-1127.
[18] S. Tsuzuki, K. Kubota, H. Matsumoto *J. Phys. Chem. B*. **2013**, *117*, 16212-16218.
[19] Y. R. Dougassa, C. Tessier, L. El Ouatani, M. Anouti, J. Jacquemin, *J. Chem. Thermodyn.* **2013**, *61*, 32-44.
[20] J. Chidiac, L. Timperman, M. Anouti, *ChemPhysChem*. **2021**, *22*, 1-18
[21] J. Pires, L. Timperman, J. Jacquemin, A. Balducci, M. Anouti *J. Chem. Thermodyn.* **2013**, *59*, 10-19.
[22] M. Li, I. Katsouras, C. Piliego, G. Glasser, I. Lieberwirth, P. W. M. Blom, D. M. de Leeuw, *J. Mater. Chem. C*. **2013**, *1*, 7695-7702.
[23] L. Glasser, *Thermochim. Acta*. **2004**, *421*, 87-93.
[24] M. Vraneš, S. Papović, A. Tot, N. Zec, S. Gadžurić, *J. Chem. Thermodyn.* **2014**, *76*, 161-171.
[25] J. K. Shah, J. F. Brennecke, E. J. Maginn, *Green Chem*. **2002**, *4*, 112-118.
[26] B. K. Xiong, M. Paillot, M. Anouti, *J. Chem. Eng. Data*. **2020**.
[27] F. S. Mjalli, *Chin. J. Chem. Eng.* **2016**, *24*, 1779-1785.
[28] X. Bogle, R. Vazquez, S. Greenbaum, A. v. W. Cresce, K. Xu, *J. Phys. Chem. Lett.* **2013**, *4*, 1664-1668.
[29] J. Jones, M. Anouti, M. Caillon-Caravanier, P. Willmann, D. Lemordant, *Fluid Phase Equilib.* **2009**, *285*, 62-68.
[30] J. Chidiac, L. Timperman, M. Anouti, *J. Energy Chem.* **2022**, *65*, 352-366.
[31] R. Macías-Salinas, *J. Mol. Liq.* **2018**, *262*, 161-174.
[32] C. Schreiner, S. Zugmann, R. Hartl, H. J. Gores, *J. Chem. Eng. Data*. **2010**, *55*, 1784-1788.

[33] B. Gorska, L. Timperman, M. Anouti, F. Beguin, *Phys. Chem. Chem. Phys.* **2017**, *19*, 11173-11186.
[34] G. Nikiforidis, W. A. Daoud, *J. Electrochem. Soc.* **2015**, *162*, A809-A819.
[35] M. Anouti, L. Timperman, *Phys. Chem. Chem. Phys.* **2013**, *15*, 6539-6548.
[36] G. Nikiforidis, M. Raghibi, A. Sayegh, M. Anouti, *J. Phys. Chem. Lett.* **2021**, *12*, 1911-1917.
[37] T. Romann, J. Eskusson, T. Thomberg, E. Lust, A. Jänes, *J. Electrochem. Soc.* **2021**, *168*, 070528.
[38] M. Zhang, W. Wang, X. Liang, C. Li, W. Deng, H. Chen, R. Li, *Chin Chem. Lett.* **2021**.
[39] S. Phadke, R. Mysyk, M. Anouti, *J. Energy Chem.* **2020**, *40*, 31-38.
[40] D. Leistenschneider, L. H. Heß, A. Balducci, L. Borchardt, *Sustain Energ Fuels*. **2020**, *4*, 2438-2447.
[41] P. Galek, E. Frackowiak, K. Fic, *Electrochim. Acta*. **2020**, *334*, 135572.

10.1002/cphc.202200224

ToC

Non-flammable, safe, and functional deep eutectic solvents based on sodium fluorosulfonyl trifluoromethanesulfonyl imide and sodium cyano-trifluoromethanesulfonyl imide with ethylene carbonate are used as electrolytes for supercapacitor applications.